COPPER ELECTROLESS DEPOSITION ON NiTi SHAPE MEMORY ALLOY : AN XPS STUDY OF Sn-Pd-Cu GROWTH

J.F. Silvain[2], S. Trombert[1], J. Chazelas[1], M. Lahaye[2], Olivier Fouassier[2]

[1]THOMSON-CSF / RCM, La Clef de St Pierre, F-78852 - ELANCOURT(FRANCE)
[2]Institut de Chimie de la Matière Condensée de Bordeaux (ICMCB) - CNRS, Université de Bordeaux I, 87 Av. du Dr. A.. Schweitzer, F-33608 - PESSAC (FRANCE)

SUMMARY : XPS analysis of electroless deposition of successive Sn, Pd and Cu films on NiTi(O) surface has been done in order to explain their nucleation and growth. Chemical interaction of Sn sensitisation element with NiTi(O) surface is shown to be associated with the growth of Sn(O) interfacial oxide which can be formed after the reaction of Sn atoms with Ni_2O_3 nickel oxide. The dissociation of this non stable oxide leads to the formation of Sn oxide film and to the migration of free metallic nickel atoms at the free surface of the electroless Sn(O) film Pd chemisorption on Sn(O) surface is associated with the formation of strong Sn-O-Pd interfacial bonds. Further on, 2D and 3D growth, of pure metallic palladium, occurs leading to the formation of nonometric Pd clusters. The interaction of copper atoms with that palladium surface leads to the formation of interfacial Pd-Cu intermetallic and consequently to strong interfacial adhesion.

KEYWORDS : Tin lead silver alloy, nickel titanium, metal matrix composite, electroless copper coating, interfacial study, X ray photoelectron spectroscopy (XPS)

INTRODUCTION

Electroless metal deposition and autocatalytic chemical processes are widely used for the growth of many metal and alloys on most of surface shapes. Due to its simple, low coast and easy to used process [1], it has been used in fields like automotive and electronics [2] for the metallisation of simple and complex metals, ceramics [3, 4] and plastics [5] substrates. This method can be used in order to obtain either thick or thin (less than 1 μm) uniform coating.
Our interest in electroless metal deposition processes are related to our research in the elaboration of metal matrix composite where micronics shape memory alloys (SMA) NiTi particles have to be introduced inside a liquid matrix. Due to the non wetting properties of NiTi with the liquid SnPb matrix, a copper thin film, which has a contact angle with liquid SnPb matrix smaller than 90° [6], is electroless deposited on NiTi substrate.

The process we first used was essentially based on the dipping of flat rectangular shape SMA NiTi substrate, at room temperature, on two successive baths. The first one was used to remove any surface oxide trace, where the second, the coating bath, was used to coat NiTi surface with copper. However, whatever the dipping time and the bath composition, copper thin film had never been successfully deposited on NiTi substrate.
In order to be able to grow electroless copper on that substrate, localised catalytic centers have to be created on the NiTi surface; they will help to initiate electroless metal deposition. These sites are constituted by palladium clusters chemisorbed on the substrate surface. Two main methods have up to now being proposed : the conventional two-step process which used , successively, dilute solutions of $SnCl_2$ and then $PdCl_2$ [7, 8, 9], and the one-step process which used a mixed $SnCl_2$-$PdCl_2$ solutions [7, 10]. The reaction should then proceeds autocatalytically to form an homogeneous metal film on the surface of the substrate. A large literature can be find on that subject [7-9, 11, 12], but the problem of the reaction mechanisms and the role of the substrate is far from being solved. In that sense, this article involves the nucleation and growth of copper on Pd-Sn-NiTi surface. The growth of electroless Sn and Pd clusters and copper films onto NiTi surface is described and a schematic nucleation and growth model is proposed.

EXPERIMENTAL

The principal results of this study aim at revealing the process of adsorption of tin and palladium on NiTi surface and the subsequent growth of copper thin films by electroless deposition method. In our experiments, the electroless process is essentially based on the dipping, at room temperature, of NiTi SMA plate in four different and successive baths [6]. a) Desoxidation bath, b) sensitisation bath : 10g/l $SnCl_2$, 40 ml/l of 38% Hcl, c) activation bath : 0.25g/l $PdCl_2$, 2.5 ml/l of 38% HCl, d) coating bath : 10g/l $CuSO_4$, 10g/l NaOH, 50g/l $KNaC_4H_4O_6.4H_2O$, 15 ml/l CHOH, where CHOH initiates the coating deposition by reducing $CuSO_4$. Between each bath, substrates are rinsed in distilled water, and, at the end of the process, carefully dried in an Ar^+ atmosphere oven at 70°C. The morphology of the coating was controlled by scanning electron microscopy (SEM). The deposition rate of each metal has been optimised with the help of a statistical design of experiments, where the modified parameters are the dipping times in each bath, and the response parameter are the residual Pd and Cu coating thickness.
X ray photoelectron spectroscopy (XPS) was used in order to investigate the tin, palladium and copper adsorption processes on the NiTi surface. Depth profile XPS measurements were undertaken using a VG ESCALAB 220 i-XL instrument, using a monochromated Al Kα radiation source (150 μm spot). In all cases the spectra were charge referenced to hydrocarbon contamination C 1s peak at a binding energy (BE) of 284.5 eV. Depth profiling was achieved by argon ion etching with 3 KeV ions. The measured sample current during the depth profiling experiment was 1 mA, and an etched area was 3 x 3 mm^2, resulting in an approximate etching rate of 0.25 nm/min. The relatively large etching area compared with that being analysed (150 μm), ensures that experimental artefacts from the side of the sputtered area or induced roughness are minimised [13]. In order to minimise any artefacts from differing sample preparation process several samples were analysed.
It should be noted that with this type of sample there are different etch rates for different metal and possible interfacial intermetallic. The relative sputter yield of the individual components of the film can lead to differences in the measured atomic concentration during a sputtering experiment. Laegrid et al. [13] showed that in their pure state the sputter yield (at 600 eV) for Ti, Ni, Pd and Cu are 0.58, 1.52, 2.39 and 2.3 respectively (no data is available

for Sn). Hence during a profiling experiment attention should be paid to the preferential sputtering of certain elements. Data were acquired for the Ti 2p (430-460 eV), Ni 2p (840-885 eV), Pd 3d (320-350 eV), Cu 2p (910-970 eV), Sn 3d (470-500 eV), O 1s (522-542 eV) and C 1s (276-294 eV) regions. Deconvolution of the spectra was achieved by fitting the data with a Gaussian/Lorentzian combination peak shape with variation in peak FWHM, position and height being determined by an iterative program. The peak identification were determined by reference to an XPS data base [14, 15] or from compounds analysed in the same apparatus. Non linear least square fitting (NLLSF) analysis of this data was required due to the conflict of several peaks of interest, for example Al 2p and Ni 3p peaks, and Fe 2p and Ni LMM Auger peaks. The Eclipse data system used on the VG ESCALAB 220 i-XL uses a NLLSF routine developed from the methodology discussed by B. Ja Ber et al. [16].

RESULTS AND DISCUSSIONS

NiTi substrate

Table 1 shows the typical evolution, after peak decomposition, of the NiTi surface sample before and after 1 min Ar^+ sputtering. Before Ar^+ sputtering, Ti, Ni, O and C signals are detected on all the studied samples. The dominant surface elements are always oxygen and carbon. It has to be noticed that all carbon peaks, located around 284.5 eV and 288.2 eV, which are assigned to C-C, C-O and C=O, respectively, disappear after the first run of sputtering in all TiNi, TiNi-Sn, TiNi-Sn-Pd and TiNi-Sn-Pd-Cu studied samples. Consequently, the contribution of carbon will be neglected in further discussions. It also has to be noticed that, a peak at 282.0 eV, characteristic to Ti-C carbide species, has never been observed on all analysed samples.

Ar^+ sputtering	C 1s	O 1s	Ni $2p_{3/2}$	Ti $2p_{3/2}$
0 s	284.5 (1.5) 9	529.9 (1.3) 46	852.4 (1.6) 25	454.3 (1.7) 10
	286.0 (1.5) 14	531.6 (2.4) 54	856.0 (2.8) 75	458.3 (1.4) 70
	288.1 (1.3) 77			459.5 (2.5) 20
1 min		529.8 (1.3) 49	853.0 (1.0) 80	454.3 (1.2) 49
		531.5 (2.2) 51	854.9 (2.4) 20	455.6 (2.4) 51

BE (eV) (FWHM (eV)) Relative area (%)

Table 1 : C1s, O1s, Ni2$p_{3/2}$ and Ti2$p_{3/2}$ BE, before and after Ar^+ sputtering, of NiTi material

Before Ar^+ sputtering, the various components of the Ni $2p_{3/2}$, Ti $2p_{3/2}$ and O 1s XPS peaks have been extracted. Two components are necessary to obtain a reasonable adjustment of the Ni $2p_{3/2}$. The lowest binding energy (BE) peak at 852.4 eV is assigned to Ni in the metallic state and the highest BE peak at 856.0 eV is assigned to Ni^{3+} that is characteristic of the Ni_2O_3 [17]. Three components were necessary to fit the Ti $2p_{3/2}$. The lowest BE peak at 454.3 eV is assigned to Ti that is characteristic of intermetallic TiNi, and the two highest one at 458.3 eV and 459.5 eV are assigned to Ti^{4+} that is characteristic of the TiO_2. However, it has been seen that in the case of half surface coverage, the BE of Ti^{4+} is slightly smaller (458.5 eV [18]) than the BE of a full substrate coverage (459.0 eV [14]). This BE difference can be relative to size and support effect in a similar way as it has been previously observed for TiO_2/SiO_2 samples. The decomposition of the O1s peak shows two components : one at high BE (531.6 eV) assigned to C=O and Ni_2O_3 and one at low BE (529.9 eV) assigned to TiO_2.

The nickel and titanium oxide evolution, after Ar^+ sputtering, are mainly due to artefact effect due to a preferential oxygen removal effect [19]. Indeed, after Ar^+ sputtering of TiO_2, TiO_x surface, with a BE close to 455.8 eV, is formed. However, in our knowledge, the evolution, after Ar^+ sputtering, of Ni^{3+} (BE = 856.0 eV) characteristic of the Ni_2O_3 oxide surface of NiTi, to Ni^{2+} (BE = 854.9 eV), characteristic of the NiO oxide, has not yet been reported in the literature. Therefore, as for TiO_2, a preferential removal of oxygen can take place in Ni_2O_3 leading to a non stoichiometric and defective surface.

NiTi-Sn substrate

The attenuation of the Ti2p and Ni2p peaks, due to Sn adsorption, ables us to determine the average Sn thickness which is close to 3 nm. This thin Sn film allowed us to analyse in the same time the top NiTi(O) surface and the free Sn tin film surface; however no evidence can be given on the growth mode (2D (continuous film growth) or 3D (cluster growth)). Nevertheless, after Ar^+ sputtering, the Ti2p and Ni2p NiTi(O) oxide evolution (cf. Table 2) shows that the NiTi(O) surface is not fully covered with Sn layer. Finally, with the help of SEM observations, we are able to conclude that most of the substrate surface is covered with an almost 2D Sn film which can be in fact associated with a strong chemical interaction between NiTi(O) surface and the Sn adsorbed atoms.

Sputter time	C 1s	O 1s	Ni $2p_{3/2}$	Ti $2p_{3/2}$	Sn $3d_{5/2}$	Cl $2p_{3/2}$
0 s	284.5 (1.2) 65	529.6 (1.3) 25	851.7 (1.1) 95	453.7 (1.4) 5	486.6 (1.3)	198.4 (1.4)
	285.9 (1.5) 25	531.4 (2.5) 70	855.7 (3.0) 5	458.1 (1.1) 95	-	-
	288.5 (1.3) 10	533.5 (0.9) 5	-	-	-	-
10 s	-	530.5 (1.2) 70	852.8 (1.1) 60	454.3 (0.8) 20	484.8 (1.0) 30	-
	-	531.5 (2.3) 30	854.1 (1.6) 40	455.0 (1.2) 20	486.8 (1.7) 70	-
	-	-	-	458.9 (1.6) 60	-	-

BE (eV) (FWHM (eV)) Relative area (%)

Table 2 : C 1s, O 1s, Ni $2p_{3/2}$, Ti $2p_{3/2}$, Sn $3d_{5/2}$ and Cl $2p_{3/2}$ BE, before and after Ar^+ sputtering, of NiTi-Sn material

Table 2 shows the typical evolution, after peak decomposition, of the NiTi-Sn surface sample before and after 10 s Ar^+ sputtering (close to the NiTi(O)/Sn interface). In order to understand how the Sn atoms can interact with the NiTi(O) substrate one, the XPS results, after Ar^+ sputtering, are discussed. As for the non sputter NiTi(O) surface, the $Ti2p_{3/2}$ peak can be decomposed in three components. The first one at low BE (454.3 eV) is assigned to Ti characteristic to TiNi and the two others, at higher BE, are assigned to Ar^+ modified TiO_x species at BE close to 455.0 eV (artefact effect) and to non Ar^+ modified TiO_2 species at BE close to 458.9 eV. It has to be noticed that the metal/oxide ratio (0.11 = 10/(70+20) (cf. Table 1) of non Ar^+ sputter TiNi(O) surface is close to the metal/oxide ratio (0.25 = 20/(60+20)) (cf. Table 2) of the surface of the sputter TiNi(O)-Sn. The oxide species, used for the calculated metal/oxide ratios, refer, respectively, to TiO_2 (70%) and non fully covered TiO_2 surface (20%) species (Table 1 before Ar^+ sputtering) and to TiO_2 (60%) and to Ar^+ modified TiO_2 (20%) species (Table 2 after Ar^+ sputtering). Consequently, we can assume that Sn atoms

present at the NiTi(O) surface does not chemically interact with the Ti(O) surface species during the thin electroless deposition process.
Similar reasoning process can be apply on the Ni2p evolution between the non sputter NiTi(O) surface and the sputter NiTi(O)-Sn interface. After Ar^+ sputtering, two components, which BE (852.8 eV and 854.1 eV) are necessary to decomposed the $Ni2p_{3/2}$ peak (cf. Table 2). However, the metal/oxide ratio difference observed, 0.33 (25/75) for NiTi(O) and 1.5 (60/40) for NiTi(O)-Sn, shows that Sn has to react with Ni_2O_3 surface oxide. The decomposition of the $Sn3d_{5/2}$ peak (after Ar^+ sputtering) shows two components at BE close to 484.8 eV and 486.8 eV and assigned respectively to Sn^0 and Sn^{2+} and/or Sn^{4+}, respectively. However, the higher Gibbs enthalpy of formation, at room temperature, of SnO_2 (ΔG = -520 KJ/mole) [20], with respect to SnO (ΔG = -257 KJ/mole) [20], lead us to suggest that the 486.7 BE measured is assigned to Sn^{4+} that is characteristic of the Sn_2O.
Table 2 shows also the decomposition of the $Cl2p_{3/2}$ peak which can be assigned to $SnCl_2$ compounds. It has to be noticed that, because of the very low Cl atomic concentration (less than 1%), Cl species will not be considered in the Pd adsorption process.
Indeed, from the XPS results, the following reaction between the surface Ni(O) oxide and the ad Sn atoms can be proposed :

$$2\ Ni_2O_3\ (NiTi(O)) + 3\ Sn \dashrightarrow 3\ SnO_2\ (interface) + 4\ Ni$$

leading to chemical interactions, at the NiTi(O) surface, between the Sn atoms and the Ni(O) oxide surface. The Sn atms, which are adsorbed on the NiTi(O) surface, are formed in the $SnCl_2$ solution after reduction of the Sn^{2+} ions by the NiTi(O) surface. The free Ni atoms, produced during this reaction, can diffuse through the Sn(O)-Sn film (during the film growth) and segregate at the free Sn surface as observed before Ar^+ sputtering in Table 2. In that way, the Ni^0 species, at BE close to 851.7, can be explained and can be correlated with the Ni(O) oxide decomposition.

NiTi-Sn-Pd substrate

Table 3 shows the typical evolution, after peak decomposition, of the NiTi-Sn-Pd surface. Before Ar^+ sputtering, Ti, Ni, Sn, Pd, O, Cl and C signals are detected on all the studied samples; therefore, the various components of the $Ni2p_{3/2}$, $Ti2p_{3/2}$, $Sn3d_{5/2}$, $Pd3d_{5/2}$, $Cl2p_{3/2}$ and O1s XPS peaks have been extracted. The decomposition of the $Ni2p_{3/2}$, $Ti2p_{3/2}$, $Sn3d_{5/2}$, and O1s peaks, which are, in fact, almost similar to the NiTi-Sn samples before Ar^+ sputtering (cf. table 2), will not be discussed. On the other hand, the evolution of the Pd species before (cf. table 3) and after (cf. table 4) Ar^+ sputtering is analysed.

Sputter time	O 1s	Ni $2p_{3/2}$	Ti $2p_{3/2}$	Sn $3d_{5/2}$	Pd $3d_{5/2}$	Cl $2p_{3/2}$
0 s	529.9 (1.6) 30	852.5 (1.8) 25	454.2 (1.8) 5	486.6 (1.3)	334.7 (0.9) 60(TF)	197.3 (1.3) 55
	531.9 (2.1) 55	855.6 (2.0) 75	458.3 (1.4) 95	-	335.4 (1.2) 40(CL)	198.9 (1.6) 45
	533.6 (1.2) 15	-	-	-	-	

BE (eV) (FWHM (eV)) Relative area (%), TF : Thin Film, CL : Cluster

Table 3 : O1s, $Ni2p_{3/2}$,$Ti2p_{3/2}$, $Sn3d_{5/2}$, $Pd2p_{5/2}$, and $Cl2p_{3/2}$ BE, before and after Ar^+ sputtering, of NiTi-Sn material

Two components, one at lowest BE (334.7 eV) assigned to Pd metallic (Pd^0) film and one at highest BE (335.4 eV) assigned to nanometric metallic Pd (Pd^0) clusters, have been found. Fristch et al [21], Nosova et al [22] and Voogt et al [23] shows that the shape difference between Pd metallic (Pd^0) film and nanometric metallic Pd (Pd^0) clusters can be associated with an increase of the $Pn3d_{5/2}$ BE. For these authors, the BE change is mainly related with the reduction of the cluster valence electrons or by relaxation effect which tends, in both explanations, to increase the BE when the cluster size decreases. Table 3 also shows the decomposition of the $Cl2p_{3/2}$ peak, at BE close to 197.3 eV and 198.9 eV. These two peaks are assigned to Pd^{2+} characteristic of the $PdCl_2$ surface compounds and to some Cl-C-O species, respectively.
As for the TiNi(O)-Sn specimens a very low Cl atomic concentration (less than 1%) is found; consequently, Cl species will not be considered in the Cu adsorption process. Table 4 shows the evolution of the $Pd3d_{5/2}$ XPS peaks with the Ar^+ sputtering time. After the first sputtering run, Pd oxide, at BE close to 336.7 eV, is evidenced; this interface oxide species give evidence of the role played by the tin oxide layer in the chemisorption of palladium atoms on this corresponding surface. After 140s of Ar^+ sputtering Pd oxide film is totally removed leading to a metal palladium cluster surface surrounding by tin oxide layer.
Fig. 1 shows a model of the growth of the different metal and oxide layers which successively appear during the electroless growth of Sn and Pd species onto NiTi(O) surface.

Sputter time	0 s	20 s	60 s	140 s
	334.7 (0.9) 60 (TF)	-	-	-
Pd $3d_{5/2}$	335.4 (1.2) 40 (CL)	335.6 (1.2) 90 (CL)	335.6 (1.2) 40 (CL)	335.8 (1.4) (CL)
	-	336.7 (1.5) 10 (O)	336.6 (1.5) 60 (O)	-

BE (eV) (FWHM (eV)) Relative area (%), TF : Thin Film, CL : Cluster, O : Oxide (PdO)

Table 4 : :Evolution of the Pd $3d_{5/2}$ signal with the sputtering time

NiTi-Sn-Pd-Cu substrate

Fig. 2 is a quantified depth profile obtained before NLLSF analysis from Sn, Pd, and Cu films electroless deposited on TiNi(O) samples. The Ni, Ti, Sn, Pd and O atomic concentration evolution with the analysed depth can be easily correlated with the previous discussion where the specific evolution of the copper layer is described in Fig. 3.

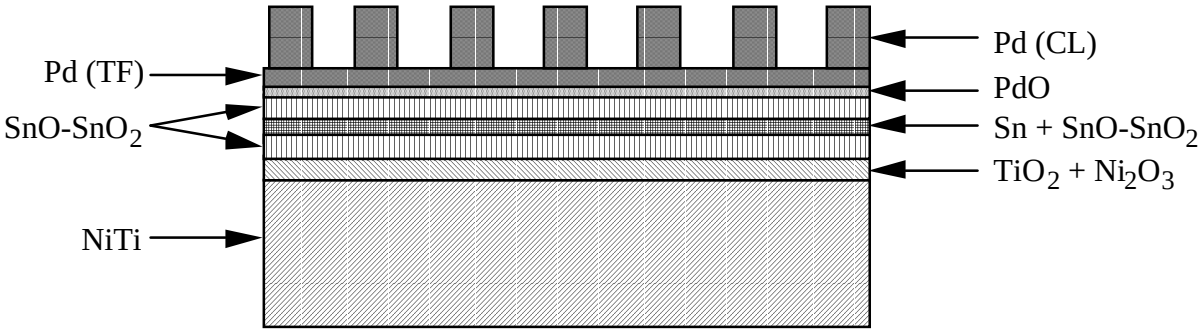

Fig. 1 : Schematic picture of the nucleation and growth of Sn + Sn(O) and Pd + Pd(O) thin film and clusters on NiTi(O) surface

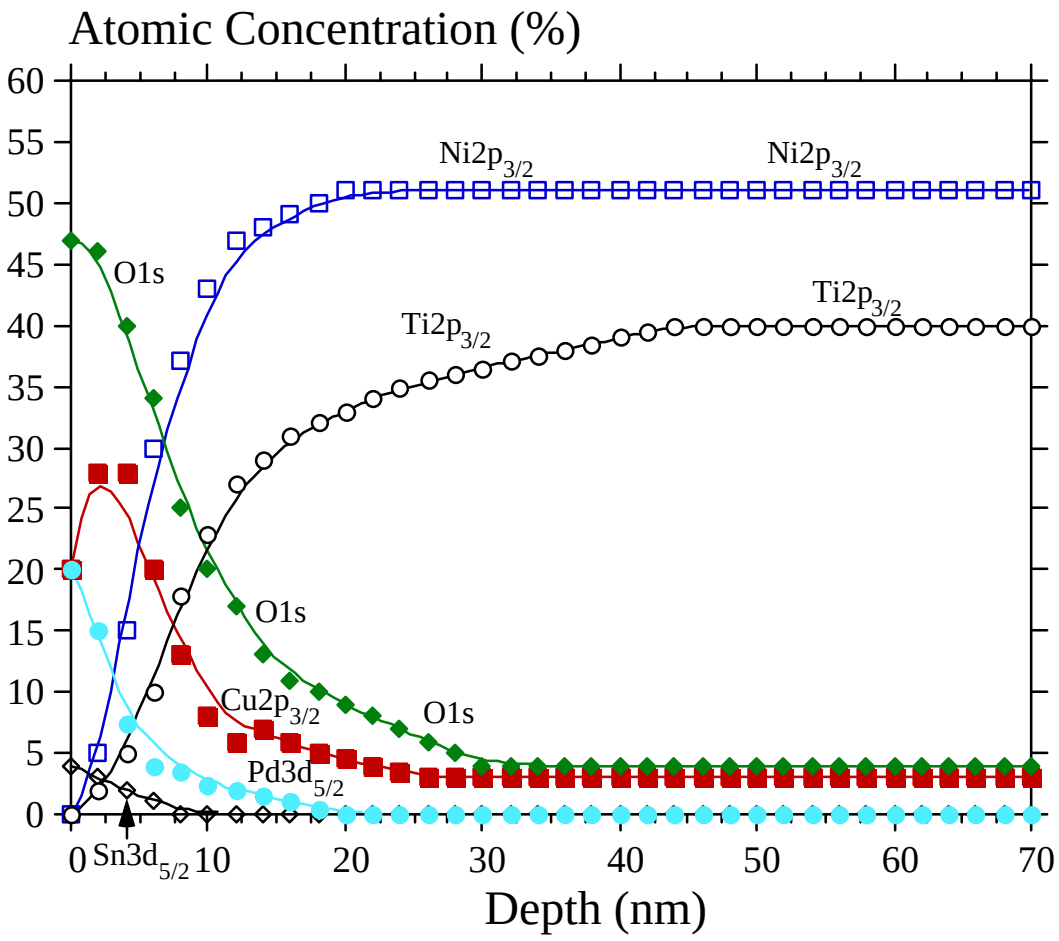

Fig. 2 : X-ray photoelectron Al Kα depth profile, obtained before NLLSF analysis, for the Ni $2p_{3/2}$, Ti $2p_{3/2}$, Sn $3d_{5/2}$, Pd $3d_{5/2}$, Cu $2p_{3/2}$ and O 1s levels of NiTi-Sn-Pd-Cu material

After NLLSF analysis, Fig. 3 shows that four copper species are present in this layer. Going from the free surface to the Pd-Cu interface the four species can be defined as follows. The first species, labelled Cu-O, can be attributed to copper oxide surface (CuO) at a binding energy, for the Cu $2p_{3/2}$, close to 933.1 eV. The second, labelled Cu metal, can be attributed to the pure metallic state at a binding energy, for the Cu $2p_{3/2}$, close to 932.6 eV. The two last species, are associated with the interface area zone, where the copper atoms react with the Pd clusters and thin film, to form Pd-Cu intermetallic compound (BE = 932.2 eV) [24] and possible Pd-Cu-O or Pd-Sn-Cu one (BE = 934.1 eV).

In that manner, the interaction of the copper ad atoms with the metallic palladium surface, is governed by the intermetallic formation of a Pd-Cu compound; consequently the chemisorption of copper ad-atoms leads to a strong adhesion between the electroless copper thin films and the NiTi(O)-Sn-Pd surface.

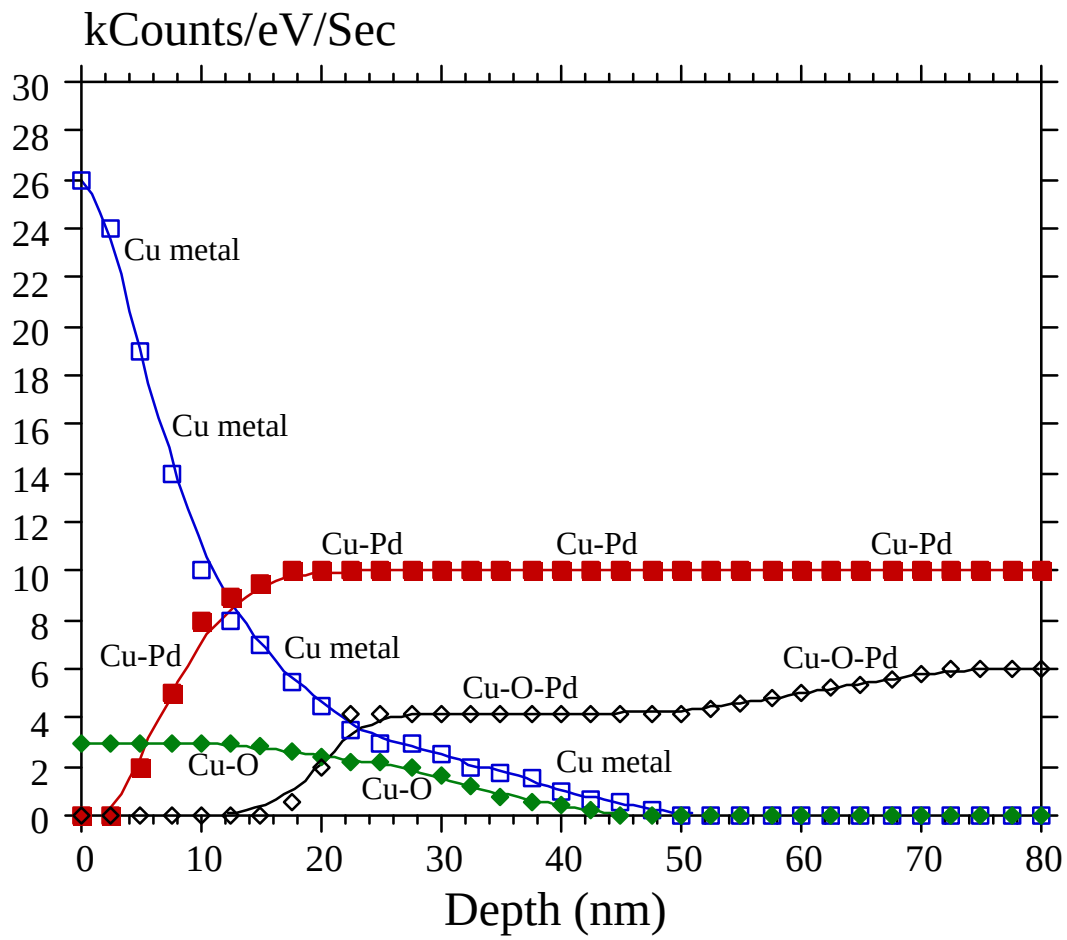

Fig. 3 : X-ray photoelectron Al Ka depth profile, obtained after NLLSF analysis, for the different Cu $2p_{3/2}$ species of NiTi-Sn-Pd-Cu material

CONCLUSIONS

XPS analysis of electroless deposition of successive Sn, Pd and Cu films on NiTi(O) surface lead us to explain how chemical interactions can take place, inside the electroless baths, between the deposited films and the different specimen surfaces. A conventional two-step process where dilute solutions of $SnCl_2$ and then $PdCl_2$ are used in order to able the nucleation and growth of copper thin film. Chemical interaction of Sn sensitisation element with NiTi(O) surface is shown to be associated with the growth of Sn(O) interfacial oxide which can be formed after the reaction of Sn atoms with Ni_2O_3 nickel oxide. The dissociation of this non stable oxide leads to the formation of Sn oxide film and to the migration of free metallic nickel atoms at the free surface of the electroless Sn(O) film. Therefore, palladium film is grown on Sn(O) oxide surface. XPS results shows that Pd chemisorption on Sn(O) surface is associated with the formation of strong Sn-O-Pd interfacial bonds. Further on, 2D and 3D growth, of pure metallic palladium, occurs leading to the formation of nanometric Pd clusters. The interaction of copper atoms with that palladium surface leads to the formation of interfacial Pd-Cu intermetallic and consequently to strong interfacial adhesion.

REFERENCES

1. J. Duruelle, “ Les techniques de l’ingénieur ”, M5 Métallurgie et traitement de Surface (1996) 1551

2. R.H. Keene, Plating and Surface Finishing Vol. 68, 1988, 22

3. S.G. Warrier, and R.Y. lin, J. Mat. Science Vol. 28, 1993, 4868

4. H.M. Cheng, B.L. Zhou, Z.G. Zheng, Z.M. Wang, and C.X. Shi, Plating and Surface Finishing Vol. 77, 1990, 130

5. M. Charbonnier, M. Alami and M. Romand, J. Apply. Electrochem. Vol. 28, 1998, 449

6. S. Trombert, J. Chazelas, M. Lahaye and J.F. Silvain, Composite Interfaces, Vol. 5, No 5, 1998, 479

7. R.L. Meek, J. Electrochem. Soc. Vol. 122, 1975, 1478

8. B.K.W. Baylis, A. Busuttil, N.E. Hedgecock and M. Schlesinger, J. Electrochem. Soc. Vol. 123, 1976, 348

9. I. Kiflawick and M. Schlesinger, J. Electrochem. Soc. Vol. 130, 1983, 872

10. M. Tsukahara, J. Met. Finish. Soc. Jpn. Vol. 23, 1972, 83

11. T. Osaka, H. Takematsu and K. Nihei, J. Electrochem. Soc. Vol. 127, 1977, 349

12. T. Hamada, Y. Kumagai, N. Koshizaki and T. Kanbe, Chem. Lett. Vol. 58, 1989, 1461

13. N. Laegrid and G.K. Wekner, J. Apply. Phys. Vol. 32(3), 1961, 365

14. D. Briggs and M.P. Seah, Practical Surface Analysis Vol.. 1 AES and XPS, Chichester : Wiley (1990)

15. J.F. Moulder, W.F. Stickle, P.E. Sobol and K.D. Bomben, "Handbook of X-Ray Photoelectron Spectroscopy", Perkin-Elmer, Eden Prairie, MN, (1992)

16. B. Ja. Ber, A.N. Raev and D.A. Zushinskiy, J. Electron Spectroscopy and Related Phenomena Vol. 68, 1994, 659-667

17. S.A. Shabalovskaya and J.W. Anderegg, J. Vac. Sci. Technol. A Vol. 13(6), 1995, 2643

18. A. Fernandez, A. Caballero, A.R. Gonzales-Elipe, Surf. Interface Anal. Vol. 18, 1992, 392

19. J.P. Espinos, A. Fernandez and A.R. Gonzales-Elipe, Surf. Sci. Vol. 295, 1993, 402

20. L.B. Pankratz, Thermodynamic Properties of Elements and Oxides. 1982, U.S. Bureau of Mines

21. A. Fritsch and P. Legare, , Surf. Sci. Vol. 161, 1985, 742

22. L.V. Nosova, M.V. Stenin, Yu.N. Nogin and Yu.A. Ryndin, Apply. Surf. Sci. Vol. 55, 1992, 43

23. E.H. Voogt, A.J.M. Mens, O.L. Gijzeman and J.W. Geus, Surf. Sci. Vol. 350, 1996, 21

24. A. Rochefort, M. Abon, P. Delichere and J.C. Bertolini, Surf. Sci. Vol. 294, 1993, 43